1	Computational framework for modeling membrane processes without process and solution
2	property simplifications
3	
4	Timothy V. Bartholomew, ^{1,2} and Meagan S. Mauter ^{1,2,3,4*}
5	
6	¹ Department of Civil and Environmental Engineering, Carnegie Mellon University, 5000 Forbes Ave.,
7	Pittsburgh, PA 15213.
8	2
9	² National Energy Technology Laboratory, U.S. Department of Energy, 626 Cochrans Mill Rd., P.O. Box
10	10940, Pittsburgh, PA 15236, USA
11	2
12	³ Department of Engineering and Public Policy, Carnegie Mellon University, 5000 Forbes Ave.,
13	Pittsburgh, PA, 15213, USA.
14	ANTIL TO GO AND
15	⁴ Wilton E. Scott Institute for Energy Innovation, Carnegie Mellon University, Pittsburgh, PA, USA.
16	*C 1 1 F 11
17	*Corresponding author: E-mail: mauter@cmu.edu Office: (412) 268-5688
18	
19	Keywords: Reverse Osmosis, Osmotically Assisted Reverse Osmosis, Forward Osmosis, Pressure
20	Retarded Osmosis, Module Scale Model

Abstract

Accurately modeling membrane processes is critical to evaluating novel process configurations, designing scalable membrane systems, informing process cost estimates, and directing future research. Most membrane process models trade accuracy for computational efficiency by employing simplified approximations of the process (i.e. no salt flux, no pressure drop) and solution properties (i.e. ideal solution, and constant density, viscosity, and diffusivity). This work presents a detailed one-dimensional finite difference model for evaluating membrane processes that avoids these common simplifications. We apply this model to quantify the error introduced by these simplifications for case studies of reverse osmosis, osmotically assisted reverse osmosis, forward osmosis, and pressure retarded osmosis. While the magnitude of error introduced by these simplifications is dependent on the case study parameters and specifications, we find that existing model formulations can underestimate or overestimate average water flux by nearly 50% for some membrane processes operating under standard conditions. Finally, we investigate the error introduced by simplified inlet-outlet models that do not solve the governing system of differential equations, and we assess the accuracy of novel inlet-outlet formulations that use a log and geometric mean, instead of the typical arithmetic mean, to represent non-linear water flux profiles.

1. Introduction

Computational models are essential to describing and predicting the performance of pressure and osmotically driven membrane based processes, but the modeling framework and embedded assumptions used to describe these membrane processes vary widely. For example, some models provide simple point estimates of water flux, while others use two and three dimensional computational fluid dynamics models to estimate membrane performance. As a result, there is often significant deviation in performance estimates between process models, and few models exhibit high experimental fidelity across a range of process conditions. Shortcomings in these performance models can obscure high impact research needs for technology development, inhibit direct comparisons between processes or process configurations, impede technology scale up from the lab and facilitate sustained research in non-competitive technologies.

Detailed one-dimensional process models relate the design, operating, state, and process variables of a membrane stage using a system of differential equations. When these models are solved for a given design and operating condition, the solution describes the profiles of variables along the membrane stage (e.g. solute concentration, flow rate, water flux, etc.) and provides estimates of the overall process performance (e.g. water recovery, average water flux, pressure drop, salt passage, etc.). These stage-level process models can also be integrated into systems-scale models to estimate and optimize other key metrics like net energy consumption and cost.⁴

These detailed process models of reverse osmosis (RO) assume that the permeate side of the membrane has a negligible impact on the driving force and solve this system of differential equations using traditional ordinary differential equation solvers (e.g. Runge-Kutta method and its modified forms).⁵ For counterflow membrane processes, such as osmotically assisted reverse osmosis (OARO),^{4,6-7} forward osmosis (FO),⁸⁻⁹ pressure retarded osmosis (PRO),¹⁰ the system of differential equations is implicit and cannot be solved with traditional differential equation solvers. Instead this system of differential equations is commonly approximated using a finite difference approach and solved using numerical methods (e.g. Newton's method and trust-region methods).¹⁰ The accuracy of the finite difference approximation is dependent on the number of finite nodes, which are typically increased until there is little change between the nth and nth plus one solutions.

In contrast to detailed process models that solve for the profiles of variables along the length of the module, simplified inlet-outlet models estimate the overall process performance by averaging the inlet and outlet values of the variables. ¹¹⁻¹² For instance, an arithmetic mean of the inlet and outlet of a variable could be used to precisely represent the average value of a variable with a linear profile. This formulation preserves the key decision variables and reduces the number of variables and equations, making it attractive for use in optimization models.

The accuracy of the arithmetic mean inlet-outlet model solution breaks down, however, if there is low fidelity between the actual and assumed linear profile of the variables along the length of the module. For example, many membrane processes exhibit non-linear water flux profiles. The average of these non-linear profiles may be more accurately represented with a log or geometric mean, where the average is more heavily weighted to the lower values. This weighting reflects the common shape of non-linear water flux profiles in membrane processes, but we are unaware of previous work applying these means to inlet-outlet modeling formulations for membrane systems.

In addition to assumptions embedded in the modeling structure, most detailed process models and simplified inlet-outlet models make several additional simplifying assumptions about the process and solution properties. Common simplifications include no salt flux across the membrane, no pressure drop across the length of the stage, ideal solution properties, and constant density, viscosity, and solute diffusion coefficient (diffusivity). While these simplifications reduce the computational demand of the models, most studies do not perform a sensitivity analysis or quantitatively assess the error introduced by these simplifications. Further, even though a more accurate representation without the common simplifications may not be essential to clarifying specific phenomenon in membrane separation processes, accurate water fluxes are important when assessing the techno-economic feasibility of membrane technologies.

The present work formulates detailed process models and simplified inlet-outlet models for RO, OARO, FO, and PRO membrane processes that do not employ common simplifications for the process and solution properties described above. We use these models to quantify the error associated with each simplification. We also investigate the effect of assumptions embedded in modeling structure by assessing the impact of the number of nodes on the accuracy of the finite difference approximation method. Finally, we propose and assess the accuracy of novel simplified inlet-outlet models that use either a log or a geometric mean, as opposed to the traditional arithmetic mean, to determine the average water flux.

2. Theory

2.1 Water and salt flux

Water and salt transport in pressure driven membrane processes are generally described by Eq. 1 and 2.

$$Jw = A(\Delta P - \Delta \pi) \tag{1}$$

$$Js = B \Delta C \tag{2}$$

Where Jw is the water flux [m³/m²-h], A is the water permeability coefficient [m/bar-h], ΔP (Pf-Pp) is the hydraulic pressure difference [bar], $\Delta \pi$ (πf - πp) is the osmotic pressure difference [bar], Js is the salt flux [kg/m²-h], B is the salt permeability coefficient [m/h], and ΔC (Cf-Cp) is the salt concentration difference [kg/m³ or g/L]. The direction of the water and salt flux is defined as from the feed (f) to the permeate (p) side. For the specified flux direction, the salt flux is positive for RO and OARO and is

negative for FO and PRO. These water and salt flux equations assume the effect of the reflection coefficient in the Spiegler-Kedem model is negligible (i.e. a value of 1), which is typical for membranes with high salt rejection and low salt permeability. It the reflection coefficient is substantially less than 1, as is common in nanofiltration membranes or solutions with poorly rejected solutes, then our model will underestimate the water flux for hydraulically driven processes (RO, OARO) and overestimate the water flux osmotically (FO, PRO) driven processes. Id, 16

113 2.2 Solution properties

114

125

128

129

130

131132

141

142

143

144

The osmotic pressure is a function of the salt concentration, as shown in Eq. 3a.

115
$$\pi = i \phi C \frac{1}{MW} R T \tag{3a}$$

116 Where π is the osmotic pressure [bar], i is the number of dissociating ions [-], ϕ is the osmotic coefficient [-], C is the salt concentration [g/L], MW is the molecular weight [g/mol], R is the gas constant [8.314E-2 117 L-bar/mol-K], and T is the temperature [K]. When the solution is assumed to be ideal, the osmotic 118 119 coefficient (ϕ) is 1. In this work, we assume the solute is NaCl and the temperature is 25°C and we account for non-ideal behavior by modeling the osmotic coefficient as a function of concentration.¹⁷ We 120 determine the osmotic coefficient function from a quadratic fit of experimental results, observing close 121 agreement (less than 1% or 0.1 bar) to a more detailed osmotic coefficient relationship presented in 122 Mistry and Lienhard 2013. 17-19 The osmotic pressure of a NaCl solution as a function of only 123 concentration is presented in Eq. 3b. 124

$$\pi = K \phi(C) C = 0.848 (3.14E-6 C^2 + 2.13E-4 C + 0.917) C$$
 (3b)

Where *K* is the lumped constants in Eq. 3a (i.e. i R T/MW) and $\phi(C)$ is the osmotic coefficient as a function of concentration.

In addition to osmotic pressure, other key solution properties are a function of salt concentration or mass fraction, including: density, viscosity, and diffusivity. The density, viscosity, and diffusivity as a function of mass fraction are shown in Eq. 4-6. We determine these relationships from polynomial fits of NaCl solution property tables. 18, 20-21 Additional details on the osmotic pressure, density, viscosity, and diffusivity are included in SI Section S1.

133
$$\rho = 756 X + 995 \tag{4}$$

134
$$\mu = 2.15E-3 X + 9.80E-4$$
 (5)

135
$$D = 153 X^4 - 122 X^3 + 30.1 X^2 - 2.00 X + 1.51$$
 (6)

Where ρ is the density [kg/m³ or g/L], μ is the viscosity [Pa-s], D is the diffusivity [1E-9 m²/s], and X is the salt mass fraction [kg of solute/kg of solution]. The salt concentration is related to the density and salt mass fraction as shown in Eq. 7.

139
$$C = \rho X = 756 X^2 + 995 X \tag{7}$$

140 2.3 Concentration polarization

The concentration and osmotic pressure difference in Eq. 1 and 2 are evaluated at the membrane interface. The qualitative relationship between the concentration at the membrane interface and bulk concentration for RO, OARO, FO, and PRO on both the feed and permeate side are shown in Figure 1. When internal and external concentration polarization are accounted for with steady state film theory, the

quantitative relationship between the feed and permeate side concentration at the membrane interface and bulk concentration are determined in Eq. 8 and 9. For all membrane processes, we assume the porous support is on the side with low pressure (i.e. permeate side for RO, OARO, and FO and feed side for PRO).

$$Cm_f = Cb_f \exp\left(\frac{Jw}{k_f}\right) - \frac{Js}{Jw} \left(\exp\left(\frac{Jw}{k_f}\right) - 1\right)$$
 (8a)

$$Cm_f = Cb_f \exp\left(Jw\left[\frac{1}{k_f} + \frac{S}{D}\right]\right) - \frac{Js}{Jw}\left(\exp\left(Jw\left[\frac{1}{k_f} + \frac{S}{D}\right]\right) - 1\right)$$
 (8b)

$$Cm_p = Cb_p \exp\left(-Jw\left[\frac{S}{D} + \frac{1}{k_p}\right]\right) + \frac{Js}{Jw}\left(1 - \exp\left(-Jw\left[\frac{S}{D} + \frac{1}{k_p}\right]\right)\right) \tag{9a}$$

$$Cm_p = Cb_p \exp\left(-\frac{Jw}{k_p}\right) + \frac{Js}{Jw}\left(1 - \exp\left(-\frac{Jw}{k_p}\right)\right)$$
 (9b)

Where Eq. 8a and 9a are valid for processes with the porous support on the permeate side (i.e. RO, OARO, and FO) and Eq. 8b and 9b are valid for processes with the porous support on the feed side (i.e. PRO). The concentrations are subscripted for the side, feed (f) and permeate (p), and location, membrane interface (m) and bulk (b). The external concentration polarization on each side is modeled with the mass transfer coefficient, k, [m/h]. We assume that internal and external concentration polarization on the permeate side is negligible for RO. The internal concentration polarization is modeled with the structural parameter, S, [m] and diffusion coefficient of the solute, D, $[m^2/s]$. These concentration polarization relationships are similar to other work on the individual processes.^{4, 22-24} However, differences may arise due to the specified direction of the salt flux. The derivations of these relationships are included in SI section S.2.

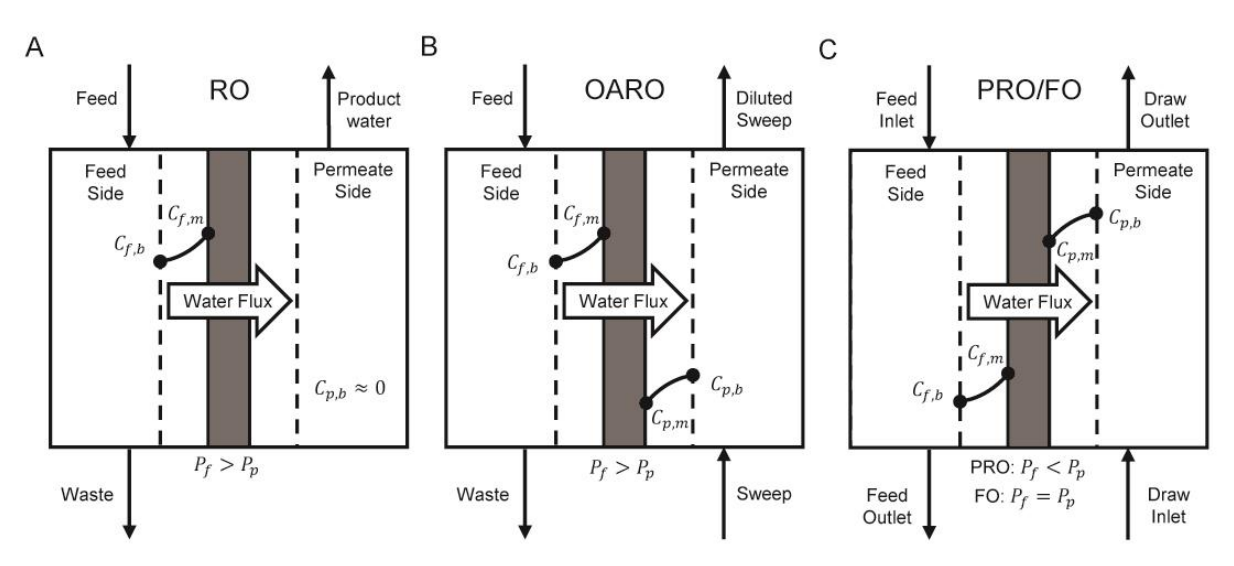


Figure 1. Schematic of process configuration and concentration polarization for A) RO, B) OARO, C) PRO/FO. The relationship between the feed and permeate-side concentration (Cf, Cp) in the bulk (b) and at the membrane interface (m) is noted within the boundary layer (dotted line). An inequality indicates whether the feed or permeate-side hydraulic pressure (Pf, Pp) is greater. We assume that the membrane porous support is on the side with the lower hydraulic pressure and on the draw-side for FO.

The mass transfer coefficient, k, is determined by Eq. 10.

$$k = \frac{D \, Sh}{d \, h} \tag{10}$$

- Where Sh is the Sherwood number [-] and d_h is the hydraulic diameter [m]. The Sherwood number is a
- dimensionless number that is a function of the Reynolds (Re) and Schmidt (Sc) number. We estimate the
- 174 Sherwood number with Eq. 11, which was developed from computational fluid dynamic simulations of
- mesh filled rectangular channels.²⁵ The definition of the hydraulic diameter is shown in Eq. 12 and is
- determined based on channel dimensions and mesh configuration as described further in SI Section S3.

$$Sh = 0.46(Re Sc)^{0.36}$$
 (11)

$$d_h = \frac{4 (flow \, area)}{(wetted \, perimeter)} \tag{12}$$

- 179 2.4 Pressure drop
- In addition to the water and salt flux, another key phenomenon is the pressure drop across the membrane stage. The pressure loss per unit length can be determined by Eq. 13.

$$PL = \frac{F \rho v^2}{2 d_h} \left[\frac{1 bar}{1E5 Pa} \right] \tag{13}$$

- Where PL is the pressure loss per unit length [bar/m], F is the friction factor [-], ρ is the fluid density
- [kg/m 3], v is the fluid velocity [m/s]. For both the pressure drop and Reynolds number calculations, the
- fluid velocity is the average axial velocity determined from the fluid flowrate, channel cross-sectional
- area, and mesh void space. F is approximated in Eq. 14 by a correlation developed for a simulated mesh
- filled channel.²⁵ The presented α and β parameters are for a filament with a circular cross section and
- effective cross-section of 25% (diameter of filament/height of channel).

189
$$F = \alpha + \frac{\beta}{Re} = 0.42 + \frac{189.3}{Re}$$
 (14)

- 190 *2.5 Governing system of equations*
- The governing system of differential equations for a one-dimensional model is composed of mass transfer and pressure drop equations shown in Eq. 15-20.

193
$$\frac{dM_f}{ds} = -(Jw \rho w + Js) W \tag{15}$$

$$\frac{d(M_f X_f)}{dz} = -Js W \tag{16}$$

$$\frac{dM_p}{dz} = (Jw \,\rho w + Js) \,W \tag{17}$$

$$\frac{d(M_p X_p)}{dz} = Js W \tag{18}$$

$$\frac{dP_f}{dz} = -PL_f \tag{19}$$

$$\frac{dP_p}{dz} = -PL_p \tag{20}$$

- Where M, X, and P are the state variables: mass flow rate [kg/h], salt mass fraction [-], and hydraulic
- pressure [bar], respectively, for the feed (f) and permeate (p) side; Jw, Js, and PL are the process
- variables: water flux [m³/m²-h or LMH], salt flux [kg/m²-h], and pressure loss [bar/m], respectively; z is

the dimension along the length of membrane [m]; and ρw is the density of water [kg/m³]. z is defined such that z=0 at the inlet (e.g. $M_f(0) = M_{f_{in}}, M_p(0) = M_{p,in}$) and z=L, the stage length, at the outlet (e.g. $M_f(L) = M_{f,out}, M_p(L) = M_{p,out}$). Note that the process variables (i.e. Jw, Js, PL) are functions of the state variables as described in the preceding section. The initial conditions of this system of differential equations are the specified inlet values for the state variables. The solution of the system of differential equations provides the profiles of the state and process variables along the stage, which can be used to extract key metrics, including: average water and salt flux, water recovery, salt passage, and feed and permeate side outlet flow rate, concentration, and pressure drop.

3. Model development

3.1 Detailed process model

We develop a detailed process model based on the finite difference approximation of the governing system of equations (Eq. 15-20). This finite difference approach discretizes the membrane stage into a series of nodes (Fig. 2). At each node, the state variables (e.g. flow rate, concentration, and pressure) and process variables (e.g. water flux, salt flux, and pressure drop) are evaluated. The process model spans the level of detail presented in section 2, where solution properties are a function of concentration and mass transfer coefficients and friction factors are determined from dimensionless numbers (e.g. Reynolds, Schmidt) that vary along the stage. The solution of this model provides the key performance metrics (e.g. average water flux, water recovery, and pressure drop) and the one-dimensional profiles of the state and process variables along the stage for a specified case.

We formulated and specified the detailed process model with the following specifications and assumptions. First, we formulate the model on a mass basis instead of a volumetric basis. The volumetric basis is the most common approach for membrane models that assume constant density. However, when density is modeled as a function of concentration, the volumetric balance does not satisfy the conservation of mass. Second, we make several assumptions that are consistent with our previous work regarding the design and operation of the membrane process.⁴ Specifically, we assume:

- The solute is NaCl and the non-ideal solution osmotic pressure matches experimental results. ¹⁷
- The membrane units have a flat plate geometry with counter-current flow and are composed of an asymmetric membrane with the porous support on the low hydraulic pressure-side.
- The mass transfer coefficient and pressure drop are adequately estimated by Sherwood number and friction factor correlations that were developed by Guillen and Hoek 2009 from simulations on channels with a mesh spacer. Despite the limitations of this study, including assumptions of constant solution properties, isolated filaments, and a Reynolds number between 10-400, these are currently the best available correlations relevant to membrane channels with a mesh.
- The continuous membrane dimensions, length and width, adequately represent a membrane stage that may be comprised of multiple modules in series and parallel.
- The outlet hydraulic pressure is 1 bar for the non-pressurized streams.

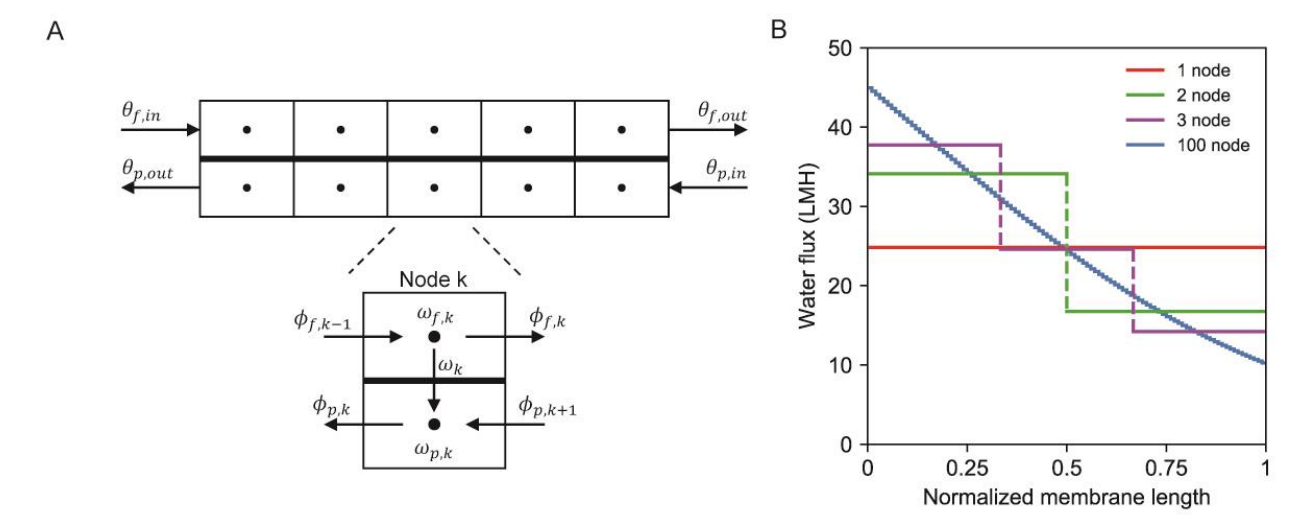


Figure 2. A) Finite difference model for hydraulic and osmotically driven membrane-based processes with five nodes. θ are inlet and outlet stage variables that include: mass flowrate, mass fraction, and hydraulic pressure. Φ are inter-node variables that include: mass flowrate, mass fraction, and pressure loss. ω are nodal variables that include: bulk concentration, concentration at the membrane interface, hydraulic and osmotic pressure, and water and salt flux. B) Water flux profiles for a different number of nodes. Water flux values are representative of the RO case study for a feed of 35 g/L TDS with 50% water recovery. Additional details are provided in Section 3.3.

The finite difference approximations of the governing mass transfer equations (Eq. 15-18) are shown in Eq. 21-32.

250
$$M_{f,k} = M_{f,k-1} - \frac{Amem}{N} (Jw_k \rho_w + Js_k) \quad \forall k, k \neq k1$$
 (21)

251
$$M_{f,k}X_{f,k} = M_{f,k-1}X_{f,k-1} - \frac{Amem}{N} Js_k \quad \forall k, k \neq k1$$
 (22)

252
$$M_{f,k1} = M_{f,in} - \frac{Amem}{N} (Jw_{k1} \rho_w + Js_{k1})$$
 (23)

253
$$M_{f,k1}M_{f,k1} = M_{f,in}X_{f,in} - \frac{Amem}{N}Js_{k1}$$
 (24)

$$M_{f,out} = M_{f,kN} \tag{25}$$

$$X_{f,out} = X_{f,kN} \tag{26}$$

256
$$M_{p,k} = M_{p,k+1} + \frac{Amem}{N} (Jw_k \rho_w + Js_k) \quad \forall k, k \neq kN$$
 (27)

257
$$M_{p,k}X_{p,k} = M_{p,k+1}X_{p,k+1} + \frac{Amem}{N} Js_k \quad \forall k, k \neq kN$$
 (28)

258
$$M_{p,kN} = M_{p,in} + \frac{Amem}{N} (Jw_{kN} \rho_w + Js_{kN})$$
 (29)

259
$$M_{p,kN}X_{p,kN} = M_{p,in}X_{p,in} + \frac{Amem}{N}Js_{kN}$$
 (30)

$$M_{n,out} = M_{n,k1} (31)$$

$$X_{p,out} = X_{p,k1} (32)$$

 Where *Amem* is the total stage membrane area and the state and process variables are either indexed by the node (k), stage inlet (in), or stage outlet (out). The set of nodes, K, has N number of nodes and is enumerated from k1 to kN, starting at the feed side inlet (permeate side outlet) and ending at the feed side outlet (permeate side inlet).

The finite difference approximations of the governing pressure drop equations (Eq. 19 and 20) are shown in Eq. 33-38. The slight difference between the mass transfer and pressure drop approximations (e.g. 1/N term in Eq. 23 compared to 1/2N term in Eq. 34) arises because hydraulic pressure is a nodal variable (w in Fig. 2) and mass flow rate and mass fraction are inter-node variables (ϕ in Fig. 2).

270
$$P_{f,k} = P_{f,k-1} - PL_{f,k-1} \frac{L}{N} \quad \forall k, k \neq k1$$
 (33)

$$P_{f,k1} = P_{f,in} - PL_{f,in} \frac{L}{2N}$$
(34)

272
$$P_{f,out} = P_{f,kN} - PL_{f,kN} \frac{L}{2N}$$
 (35)

273
$$P_{p,k} = P_{p,k+1} - PL_{p,k+1} \frac{L}{N} \quad \forall k, k \neq kN$$
 (36)

274
$$P_{p,kN} = P_{p,in} - PL_{p,in} \frac{L}{2N}$$
 (37)

275
$$P_{p,out} = P_{p,k1} - PL_{p,k1} \frac{L}{2N}$$
 (38)

In the following model description, we frequently use functions (f_*) that relate the specified variable to other variables (e.g. the osmotic pressure as a function of concentration is represented by $f_{\pi}(C)$). Previously described functions include: $f_{\pi}(C)$ as Eq. 3, $f_{\rho}(X)$ as Eq. 4, $f_{\mu}(X)$ as Eq. 5, $f_{D}(X)$ as Eq. 6, $f_{C}(X)$ as Eq. 7, $f_{Cm_{f}}(Cb_{f},Jw,Js,k_{f},D)$ as Eq. 8, and $f_{Cm_{p}}(Cb_{p},Jw,Js,k_{p},D)$ as Eq. 9.

Additionally, functions for the mass transfer coefficient (f_k) , pressure loss per unit length (f_{PL}) , and Reynolds number (f_{Re}) are formulated for the variables considered in our model, as shown in Eq. 39-41.

282
$$f_k(X, Re, Sc) = \frac{f_D(X)}{d_h} 0.46 (Re Sc)^{0.36}$$
 (39)

283
$$f_{PL}(M, X, Re, W) = \frac{\left(0.42 + \frac{189.3}{Re}\right)M^2}{2 d_h f_{\rho}(X) H^2 W^2 \varepsilon^2} \left[\frac{1 h}{3600 s}\right]^2 \left[\frac{1 bar}{1E5 Pa}\right]$$
(40)

284
$$f_{Re}(M, X, W) = \frac{M d_h}{f_{\mu}(X) H W \varepsilon} \left[\frac{1 h}{3600 s} \right]$$
 (41)

285 Where ε is the void space of the mesh filled channel (assumed to be 97% for consistency with the 286 Sherwood number and friction factor assumptions).

The nodal variables (ω in Fig. 2): water flux, salt flux, osmotic pressure, concentration at the membrane interface, bulk concentration, mass transfer coefficient, and diffusivity are determined with Eq. 42-57.

290
$$Jw_k = A((P_{f,k} - P_{p,k}) - (\pi_{f,k} - \pi_{p,k})) \quad \forall k$$
 (42)

$$Js_k = B(Cm_{f,k} - Cm_{p,k}) \quad \forall k$$
 (43)

$$\pi_{s,k} = f_{\pi}(\mathcal{C}m_{s,k}) \quad \forall s \in (f,p), \forall k$$

$$\tag{44}$$

293
$$Cm_{s,k} = f_{Cm_s}(Cb_{s,k}, Jw_k, Js_k, k_{s,k}, D_{s,k}) \ \forall s \in (f, p), \forall k$$
 (45)

294
$$Cb_{f,k} = \frac{f_C(X_{f,k}) + f_C(X_{f,k-1})}{2} \quad \forall k, k \neq k1$$
 (46)

295
$$Cb_{f,k1} = \frac{f_C(X_{f,in}) + f_C(X_{f,k1})}{2}$$
 (47)

296
$$Cb_{p,k} = \frac{f_C(X_{p,k}) + f_C(X_{p,k+1})}{2} \quad \forall k, k \neq kN$$
 (48)

297
$$Cb_{p,kN} = \frac{f_C(X_{p,in}) + f_C(X_{p,kN})}{2}$$
 (49)

298
$$k_{f,k} = \frac{f_k(X_{f,k},Re_{f,k},Sc_{f,k}) + f_k(X_{f,k-1}Ref_{k-1},Scf_{k-1})}{2} \quad \forall k, k \neq k1$$
 (50)

299
$$k_{f,k1} = \frac{f_k(X_{f,in}, Re_{f,in}, Sc_{f,in}) + f_k(X_{f,k}, Re_{f,k}, Sc_{f,k})}{2}$$
 (51)

300
$$k_{p,k} = \frac{f_k(X_{p,k}, Re_{p,k}, Sc_{p,k}) + f_k(X_{p,k+1}, Re_{p,k+1}, Sc_{p,k+1})}{2} \quad \forall k, k \neq kN$$
 (52)

301
$$k_{p,kN} = \frac{f_k(X_{p,in}, Re_{p,in}, Sc_{p,in}) + f_k(X_{p,kN}, Re_{p,kN}, Sc_{p,kN})}{2}$$
 (53)

302
$$D_{f,k} = \frac{f_D(X_{f,k}) + f_D(X_{f,k-1})}{2} \quad \forall k, k \neq k$$
 (54)

303
$$D_{f,k1} = \frac{f_D(X_{f,in}) + f_D(X_{f,k1})}{2}$$
 (55)

304
$$D_{p,k} = \frac{f_D(X_{p,k}) + f_D(X_{p,k+1})}{2} \quad \forall k, k \neq kN$$
 (56)

305
$$D_{p,kN} = \frac{f_D(X_{p,in}) + f_D(X_{p,kN})}{2}$$
 (57)

Where the subscript s denotes either the feed (f) or sweep (s) side. Note that the bulk concentration, the mass transfer coefficient, and the solute diffusion coefficient (nodal variables) are determined from the average of their functions evaluated at the adjacent inter-node variables.

The inter-node variables (ϕ in Fig. 2): pressure loss per unit length, Reynolds number, and Schmidt number are determined with Eq. 58-60.

311
$$PL_{s,u} = f_{PL}(M_{s,u}, X_{s,u}, Re_{s,u}, W) \quad \forall s \in (f, p), \forall u \in (K, in)$$
 (58)

312
$$Re_{s,u} = f_{Re}(Mf_u, Xf_u, W) \quad \forall s \in (f, p), \forall u \in (K, in)$$
 (59)

313
$$Sc_{s,u} = \frac{f_{\mu}(X_{s,u})}{f_{\rho}(X_{s,u})f_{D}(X_{s,u})} \quad \forall s \in (f,p), \forall u \in (K,in)$$
 (60)

Previously described stage level variables: membrane area, length, and width are related by Eq. 61. Other stage level variables include: average water flux (Jw_{avg}) , average salt flux (Js_{avg}) , water recovery (Rw), salt passage (Rs), and pressure drop on the feed and permeate side $(\Delta P_f, \Delta P_p)$. These variables are determined in Eq. 62-66.

$$Amem = W L \tag{61}$$

$$Jw_{avg} = \frac{1}{N} \sum_{k} Jw_{k} \tag{62}$$

$$Js_{avg} = \frac{1}{N} \sum_{k} Js_{k}$$
 (63)

$$Rw = \frac{Jw_{avg} Amem}{M_{f,in} \left(1 - X_{f,in}\right)} \tag{64}$$

$$Rs = \frac{Js_{avg} Amem}{M_{f,in} X_{f,in}}$$
 (65a)

$$Rs = \frac{-Js_{avg} Amem}{M_{p,in} X_{p,in}}$$
 (65b)

$$\Delta P_s = P_{s,in} - P_{s,out} \quad \forall s \in (f,p) \tag{66}$$

Where Eq. 65a is valid for processes with positive salt flux (i.e. RO and OARO) and Eq. 65b is valid for processes with negative salt flux (i.e. FO and PRO). Note that water recovery is defined as the fraction of permeated water mass flow rate over the feed inlet water mass flow rate, as opposed to the inlet feed volume reduction, which is commonly used in literature. An issue with the volumetric reduction definition of water recovery is that it determines the solution recovery rather than the water recovery. The deviation between the mass and volumetric-based water recovery is small when the initial feed concentration is dilute, but they deviate at higher salinities that are common for OARO and FO.

3.2 Simplified inlet-outlet model

The detailed process model can be simplified to an inlet-outlet model. This approach reduces the dimension of the model from one to zero by disregarding the governing system of differential equations. Instead, the inlet-outlet model estimates the overall performance of the membrane process by averaging variables at the inlet and outlet of the stage. The inlet-outlet model is computationally leaner because it has significantly fewer variables and constraints; however, its solutions are less detailed and accurate (i.e. no profiles of variables along the membrane stage).

In this work, we consider three inlet-outlet model formulations that estimate the average with: 1) the arithmetic mean, 2) the log mean, and 3) the geometric mean. These means are specified in Eq. 67a, 67b, and 67c, respectively. We approximate the log mean with an approximation developed by Chen 1987 because the log mean can be undefined over the domain of feasible variables.²⁶⁻²⁷

344
$$f_{avg}(Y_1, Y_2) = \frac{(Y_1 + Y_2)}{2}$$
 (67a)

345
$$f_{avg}(Y_1, Y_2) = \frac{Y_1 - Y_2}{\ln(\frac{Y_1}{Y_2})} \approx \left(Y_1 Y_2 \frac{(Y_1 + Y_2)}{2}\right)^{\frac{1}{3}}$$
 (67b)

346
$$f_{avg}(Y_1, Y_2) = (Y_1 Y_2)^{\frac{1}{2}}$$
 (67c)

The mass balance and pressure drop equations around the membrane stage are shown in Eq. 68-348 72.

$$M_{f,out} = M_{f,in} - Amem(Jw_{avg} \rho_w + Js_{avg})$$
 (68)

$$M_{f,out} X_{f,out} = M_{f,in} X_{f,in} - Amem J s_{avg}$$
 (69)

$$M_{p,out} = M_{p,in} + Amem(Jw_{avg} \rho_w + Js_{avg})$$

$$\tag{70}$$

$$M_{p,out} X_{p,out} = M_{p,in} X_{p,in} + Amem J s_{ava}$$

$$(71)$$

$$P_{s,out} = P_{s,in} + PL_{s,ava} L \quad \forall s \in (f,p)$$
 (72)

The averaged process variables Jw_{avg} , Js_{avg} , and $PL_{s,avg}$ are determined in Eq. 73-75.

$$Jw_{ava} = f_{ava}(Jw_1, Jw_2) (73)$$

$$Js_{avg} = \frac{Js_1 + Js_2}{2} \tag{74}$$

$$PL_{s,avg} = f_{avg}(PL_{s,in}, PL_{s,out})$$
(75)

Where f_{avg} is Eq. 67a, 67b, or 67c depending on the mean formulation, the numbered subscript denotes the membrane stage end: 1 for feed side inlet and permeate side outlet, and 2 for feed side outlet and permeate side inlet. We determine the average salt flux using the arithmetic mean for all inlet-outlet models since we observe nearly constant or linear salt flux profiles from our detailed one-dimensional model.

The water flux, salt flux, and pressure loss are determined at each end of the membrane stage with Eq. 76-80.

365
$$Jw_1 = A\left(\left(P_{f,in} - P_{p,out} \right) - \left(\pi_{f,in} - \pi_{p,out} \right) \right)$$
 (76)

366
$$Jw_2 = A\left(\left(P_{f,out} - P_{p,in} \right) - \left(\pi_{f,out} - \pi_{p,in} \right) \right)$$
 (77)

$$Js_1 = B\left(Cm_{f,in} - Cm_{p,out}\right) \tag{78}$$

$$Js_2 = B\left(Cm_{f,out} - Cm_{p,in}\right) \tag{79}$$

$$PL_{s,u} = f_{PL}(M_{s,u}, X_{s,u}, Re_{s,u}, W) \quad \forall s \in (f, p), \forall u \in (in, out)$$

$$\tag{80}$$

All other variables, including: osmotic pressure, concentration at the membrane interface, bulk concentration, mass transfer coefficient, Reynolds number, and Schmidt number are determined in Eq. 81-89.

373
$$\pi_{s,u} = f_{\pi}(Cm_{s,u}) \quad \forall s \in (f,p), \forall u \in (in,out)$$
 (81)

374
$$Cm_{f,in} = f_{Cm_f}(Cb_{f,in}, Jw_1, k_{f,in}, D_{f,in})$$
 (82)

$$Cm_{f,out} = f_{Cm_f}(Cb_{f,out}, Jw_2, k_{f,out}, D_{f,out})$$
(83)

376
$$Cm_{p,in} = f_{Cm_p}(Cb_{p,in}, Jw_2, k_{p,in}, D_{p,in})$$
 (84)

$$Cm_{p,out} = f_{Cm_p} \left(Cb_{p,out}, Jw_1, k_{p,out}, D_{p,out} \right)$$
(85)

378
$$Cb_{s,u} = f_C(X_{s,u}) \quad \forall s \in (f,p), \forall u \in (in,out)$$
 (86)

379
$$D_{s,u} = f_D(X_{s,u}) \quad \forall s \in (f,p), \forall u \in (in,out)$$
 (87)

$$Re_{s,u} = f_{Re}(Mf_u, Xf_u, W) \quad \forall s \in (f, p), \forall u \in (in, out)$$
(88)

$$Sc_{s,u} = \frac{f_{\mu}(X_{s,u})}{f_{\rho}(X_{s,u})D_{s,u}} \quad \forall s \in (f,p), \forall u \in (in,out)$$

$$\tag{89}$$

The inlet-outlet model uses the same equations as the detailed process model (Eq. 61 and 64-66) for the stage level variables.

3.3 Case studies

 We apply our detailed process model and inlet-outlet models to case studies for RO, OARO, FO, and PRO membrane technologies. The membrane properties (Table 1) were estimated from the literature. 12, 28-30 The case study specifications (Table 1) were selected for representativeness and ease of comparison with similar process modeling exercises. 4, 8, 10, 12 In addition to the values defined by the case studies, we also perform a Monte Carlo analysis to assess the sensitivity of our results to the specified parameters. In the Monte Carlo simulations, we develop a set of 100 cases that are created by randomly sampling the parameters between +/-5% of the specified case study value.

Table 1. Case study parameter specifications. Not applicable (NA) and not specified (NS) variables are noted. We assume a basis of 1000 kg/h of feed side inlet mass flowrate. The permeate side inlet mass flowrate is determined with its mass flowrate fraction defined as $Mp_{in}/(Mp_{in} + Mf_{in})$. Specifications that are varied in the Monte Carlo analysis are noted with $\pm 5\%$.

	RO	OARO	FO	PRO
Membrane and module properties				
Water permeability coefficient [1E-12 m Pa ⁻¹ s ⁻¹]	$4.2 \pm 5\%$ [12]	$1.0 \pm 5\%$ [²⁸]	$3.2 \pm 5\% [^{29}]$	$6.9 \pm 5\% [^{30}]$
Salt permeability coefficient [1E-8 m s ⁻¹]	$3.5 \pm 5\%$ [12]	$7.7 \pm 5\%$ [²⁸]	13 ±5% [²⁹]	$11 \pm 5\% [^{30}]$
Structural parameter [µm]	NA	1200 ±5% [⁴]	$500 \pm 5\% [^{29}]$	$560 \pm 5\% [^{30}]$
Inlet specifications				
Feed side inlet mass flowrate [kg h ⁻¹]	1000	1000	1000	1000
Feed side inlet concentration [g L ⁻¹]	$35 \pm 5\%$	75 ±5%	35 ±5%	$2.9 \pm 5\%$
Feed side inlet pressure [bar]	$70 \pm 5\%$	65 ±5%	NS	NS
Permeate side inlet mass flowrate fraction [-]	0	$0.33 \pm 5\%$	$0.33 \pm 5\%$	$0.5 \pm 5\%$
Permeate side inlet concentration [g L ⁻¹]	0	100 ±5%	175 ±5%	35 ±5%
Permeate side inlet pressure [bar]	NS	NS	NS	13 ±5%
Outlet specifications				
Feed side outlet pressure [bar]	NS	NS	1	1
Permeate side outlet pressure [bar]	1	1	1	NS
Additional specifications				
Water recovery [%]	50 ±5%	50 ±5%	50 ±5%	50 ±5%
Feed side inlet Reynolds number [-]	400 ±5%	400 ±5%	400 ±5%	300 ±5%
Channel height [mm]	1 ±5%	2 ±5%	2 ±5%	2 ±5%

3.4 Solving the models

The size of the detailed process model is dependent on the number of nodes (N): 24N+27 variables, and 24N + 19 equality constraints. The simplified inlet-outlet model has 53 variables and 45 equality constraints. Both models have 8 degrees of freedom, which are reduced to zero with the case study specifications in Table 1. We create the models in Python using the open source software package Pyomo and solve for the single feasible solution using GAMS 24.5.6/CONOPT3. Additional details on bounding and initializing the variables is provided in SI Section S4.

4. Results and Discussion

This work systematically evaluates the accuracy implications of common simplifications adopted in RO, OARO, FO, and PRO membrane process models. We begin by assessing the effect of the number of nodes on the results of the finite difference approximation for water flux. We then evaluate the effect of common simplifications used in describing the process and solution properties by quantifying the difference in average water flux with and without implementation of these simplifications. Finally, we quantify the average water flux error that originates from the use of simplified inlet-outlet modeling and evaluate the performance of novel inlet-outlet model formulations that use the log and geometric means to estimate the average water flux and pressure loss.

4.1 Detailed process model results

The detailed process model with 100 nodes is solved in less than 2 seconds when using an Intel i7 CPU 2.6 GHz processor with 8 GB of memory for each of the four membrane processes. While we obtain short solution times with the solver CONOPT, the largest benefit of the commercial solver is that

the solution is tractable with crude variable bounds and initialization (SI Section S4). This solver performance contrasts with the Matlab nonlinear systems of equations solver, fsolve, which was unable to converge on a solution for the same bounds and initialization.

The solutions to the optimal process specifications and performance metrics, including average water and salt flux; salt recovery; membrane area; and feed and permeate side pressure drop, outlet concentration, average Reynolds number, and average mass transfer coefficient are reported in Table 2. We observe that our process model results are consistent with expected modeling results for the outlet concentrations, average water flux, and pressure drop.^{4, 8, 10, 12}

Table 2. Detailed process model results for the RO, OARO, FO, and PRO case studies.

Key variables and performance metrics	RO	OARO	FO	PRO
Average water flux [L m ⁻² h ⁻¹]	25.6	3.0	6.1	4.5
Average salt flux [g m ⁻² h ⁻¹]	8.1	17.4	-3.1	-6.6
Salt passage [%]	0.5	4.0	0.3	2.2
Feed side pressure drop [bar]	1.5	1.9	0.9	0.5
Permeate side pressure drop [bar]	NA	1.7	0.9	1.0
Feed side outlet concentration [g L ⁻¹]	69	131.5	69.8	7.3
Permeate side outlet concentration [g L ⁻¹]	0.3	52.9	84.1	22.7
Membrane area [m²]	19	155	80	112
Membrane width [m]	1.2	1.1	1.2	1.7
Membrane length [m]	16	141	68	67
Feed side average Reynolds number	272	273	297	226
Permeate side average Reynolds number	NA	274	261	359
Feed side average mass trans. coef. [mm h ⁻¹]	113	58	58	52
Permeate side average mass trans. coef. [mm h ⁻¹]	NA	57	58	62

The detailed process model also provides the profile of each variable along the length of the membrane, with feed concentration, permeate concentration, and water flux plotted in Figure 3. In RO and OARO, we observe the characteristically steep water flux decline along the membrane length that results from the pressure drop and the increasing feed side concentration, and in OARO, from the dilution of the sweep. In contrast, we observe a modest water flux increase from the feed inlet to the feed outlet for FO and PRO.

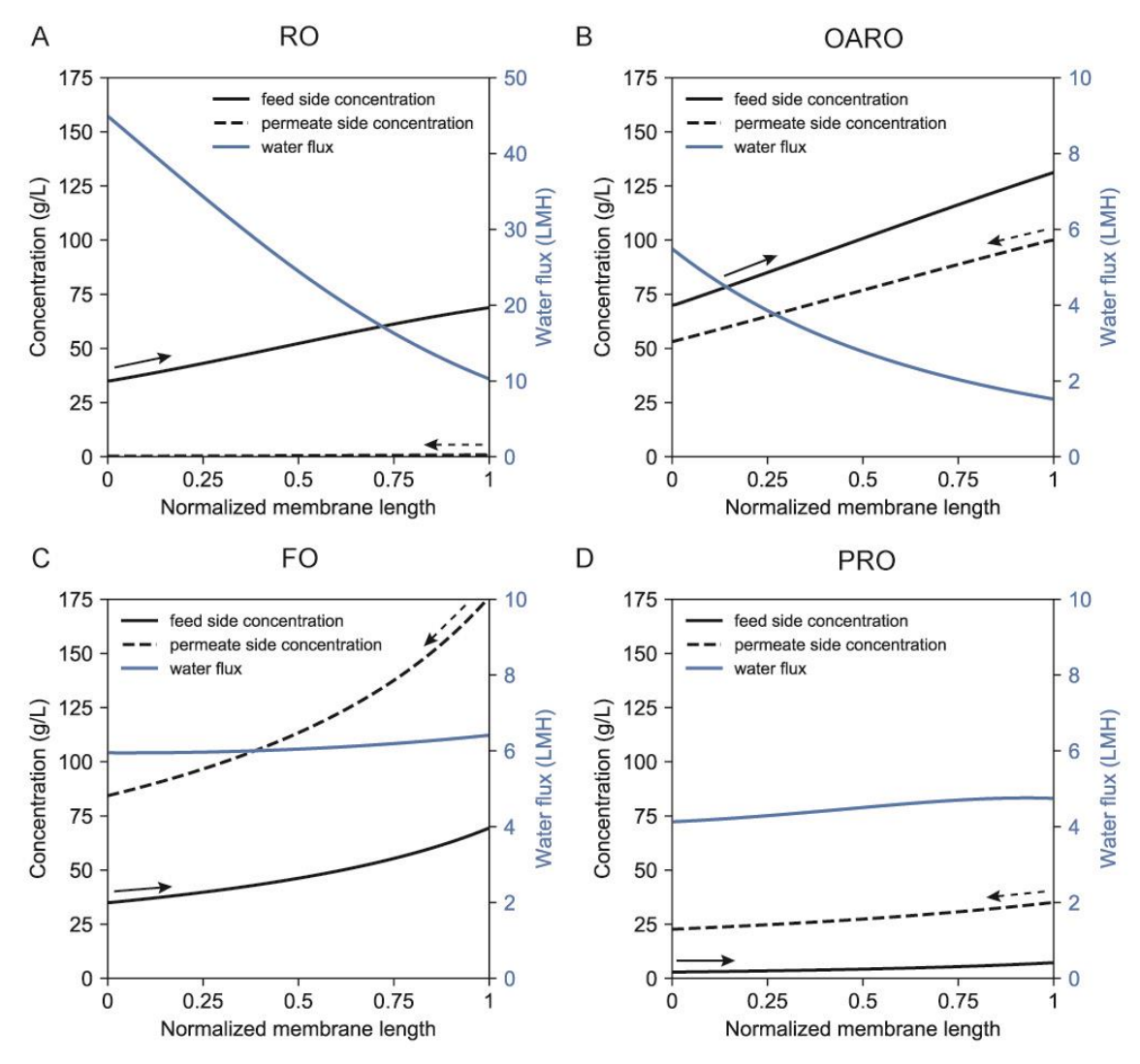


Figure 3. Bulk concentration (black) and water flux (blue) profiles along the stage for the 100 node finite difference model case studies: A) RO, B) OARO, C) FO, and D) PRO. The feed side (solid) and permeate side (dotted) concentrations are noted with line style and the flowrate directions for the streams are noted with arrows. The case study specifications and parameters are described in Section 3.3 and Table 1. Note that the RO water flux has a different scale than the other processes.

The fidelity between the detailed process model outputs and experimental measurements will depend upon the accuracy of the underlying assumptions. As noted above, the model assumes that the membranes are configured in a flat plate geometry, modules are operated in counter-current flow, friction factors and mass transfer coefficients can be described with correlations from a simulated computational fluid dynamic model, and the membrane parameters (e.g. A, B, and S) are independent of operating variables (e.g. feed and sweep side pressure and concentration). Thus, this model will not accurately describe membrane modules with different geometries (e.g. spiral wound or hollow fiber), cross flow operation, and large dead zones. We expect that our assumed flat plate geometry with only one membrane active layer bordering the flow will have longer modules than spiral wound (2 layers) or hollow fiber modules and that our assumed counter-current flow operation will have a higher average permeate-side concentration compared to the more common cross flow operation for RO processes. Finally, our model does not reflect the greater pressure drop that is expected on the low hydraulic pressure side of OARO

and PRO processes due to the lack of experimental data and friction factor correlations for those conditions.

4.2 Accuracy implications of decreasing the number of nodes in the finite difference approximation.

We assess the accuracy implications of decreasing the computational intensity of the finite difference model by decreasing the number of model nodes. In Figure 4, we plot the average difference in water flux between the n node approximation and the 100 node approximation. For each approximation, we use a Monte Carlo simulation that perturbs the specified inlet variables by $\pm 5\%$, as described in Section 3.3, to assess the sensitivity of the average water flux error to the specified conditions.

We observe that the 1 node approximation deviates from the 100 node approximation of average water flux by less than 11% for each membrane process. As the number of nodes increases, the deviation decreases to less than 1% and 0.1% for 5 and 10 nodes, respectively. Deeming 0.1% accuracy sufficient for our current work, we use the 10 node approximation for all subsequent simulations.

Generally, deviations tend to increase with decreasing driving force and increasing membrane area, as low node approximations are less accurate at representing the profile of long modules. Whether the average water flux is over or underestimated is highly dependent on the case study parameters, and we observe that even the relatively small perturbation of $\pm 5\%$ can result in either an over or underestimate for RO and PRO.

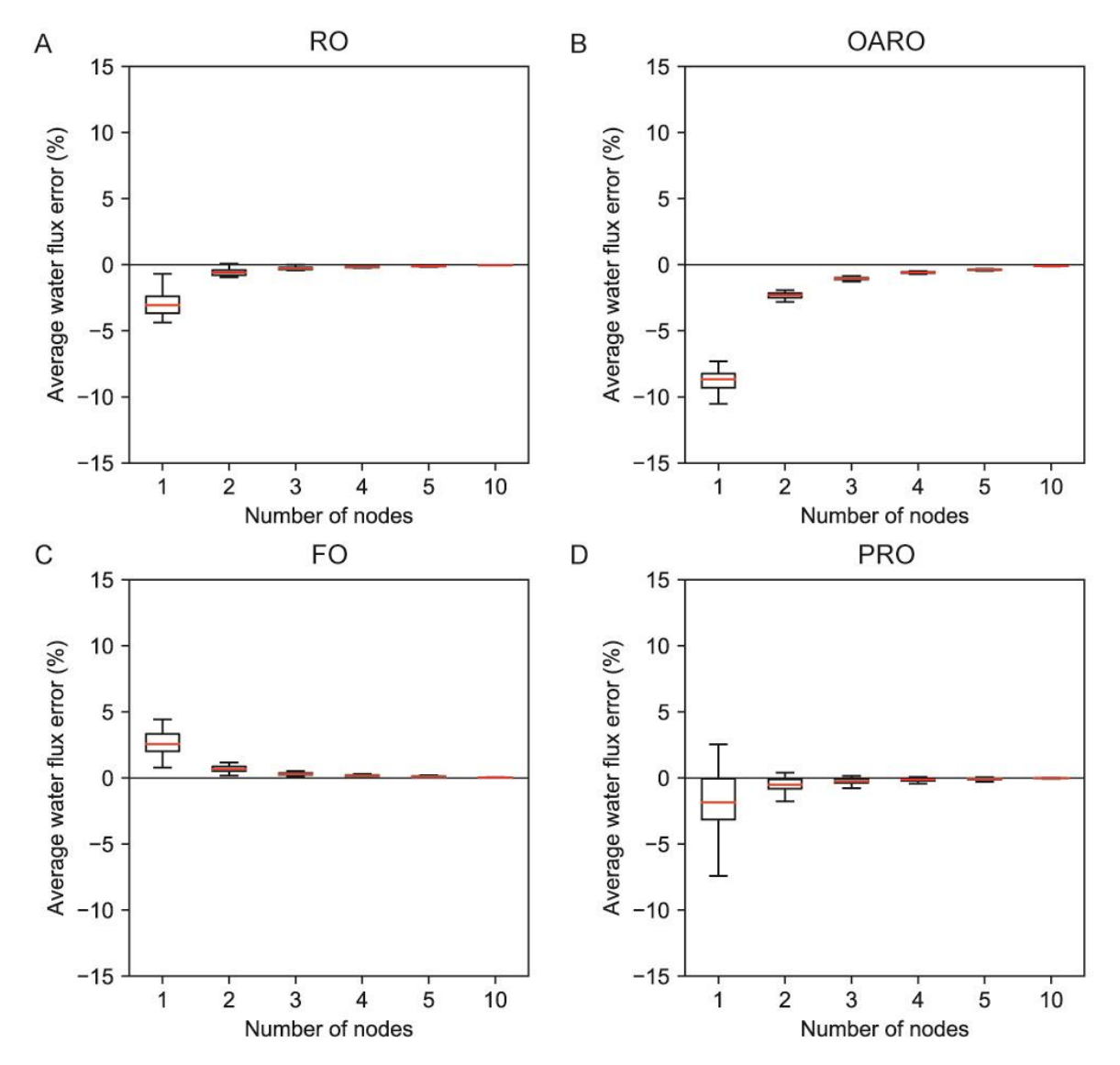


Figure 4. Accuracy of the n-node finite difference model relative to the 100 node model for A) RO, B) OARO, C) FO, and D) PRO. The water flux solution for the 100 node model is assumed to be the true value because there is an undetectable change (less than 0.001%) associated with a further increase in the number of nodes. The distribution of average water flux errors was developed using a Monte Carlo simulation that varied the specified parameters by $\pm 5\%$, as noted in Table 1.

4.3 Effect of process and solution property simplifications on model accuracy

We determine the average water flux percent error for common modeling simplifications, including: no salt flux, no pressure drop, ideal solution, and constant density, viscosity, and diffusivity for the 10 node case (Figure 5). We find that the simplifications result in water flux errors in our case studies of up to 20% for RO, 30% for OARO, 10% for FO, and 40% for PRO.

The no salt flux simplification can result in large errors (>30%) for osmotically driven membrane processes. In these processes, salt flux has a large effect on the interfacial solute concentration and therefore on the osmotic driving force. In RO and OARO, the no salt flux simplification artificially increases the interfacial solute concentration on the feed side and decreases the concentration on the

permeate side, decreasing the overall driving force and leading to an underestimation of average water flux. The inverse is true for both FO and PRO processes, which exhibit negative salt flux. Note that the no salt flux simplification results in significantly smaller errors in FO than in PRO because 1) the FO case study resulted in a lower average salt flux (Table 2), and 2) the orientation of the porous support on the permeate side in the FO case study reduces the feed side concentration polarization, which dampens the effect of assuming no salt flux.

The no pressure drop simplification results in large errors (up to 30%) for PRO and small errors (<10%) for the other membrane processes. We observe a large error for the PRO case study because neglecting the pressure drop decreases the overall driving force. When pressure drop is included, the inlet feed side pressure is greater than 1 bar and the outlet permeate side pressure is less than the specified permeate side inlet pressure. The pressure drop therefore increases the driving force at the end of the membrane stage with the feed inlet.

In contrast, when pressure drop is included for RO and OARO, the driving force decreases along the membrane length. If RO and OARO are operated at higher Reynolds numbers than those specified in our case study, the associated error with neglecting pressure drop would increase. We observe the smallest error from the no pressure drop simplification for FO because, while including the pressure drop increases the driving force at the feed inlet, it also decreases the driving force at the feed outlet and mitigates the change in average driving force along the stage. While this work only assesses the error on the average water flux, neglecting the pressure drop could result in large errors in the estimated energy consumption (or production, in the case of PRO) of the membrane processes.

The ideal solution simplification results in larger errors (>10%) for RO and PRO modeling and small errors (<5%) for RO and FO. OARO and FO are less impacted by the ideal solution assumption because the error in the osmotic pressure calculation occurs on both the feed and permeate side, effectively mitigating the net error. In contrast, the error in RO and PRO is large because only one side has a significant amount of osmotic pressure. This finding is especially significant because low concentration feeds are often used to justify the use of the ideal solution simplification in RO and PRO models.

The constant density assumption results in moderate errors (5-10%) for RO, OARO, FO, and PRO. Even though the density does not change by more than 5% between the inlet and outlet of each stream in the case studies, the constant density assumption results in moderate errors because assuming constant density leads to underestimates of the change in concentration. The magnitude of this error is directly related to the concentrations of the feed and permeate streams, with OARO and FO having the highest concentrations and the highest errors.

The constant viscosity assumption results in negligible errors (<2%) for all processes, despite the large viscosity change of over 50% across the solubility of NaCl. While viscosity has a proportional effect on the Reynolds number, it does not significantly affect the overall driving force when operating the membrane system at typical flow velocities.

The constant diffusivity assumption results in negligible errors (<0.1%) for all processes. This finding is unsurprising given that diffusivity has a limited effect on the average water flux and only varies by 10% across the solubility of NaCl at 25 °C. For processes with depressed, elevated, or non-constant temperatures, the constant diffusivity assumption may contribute to higher average water flux errors.

The cumulative error of these simplifications depends upon the process and the case study specifications. For RO and OARO, the cumulative error is less than the maximum error from a single simplification because some simplifications result in an overestimation of flux, while others result in

underestimation. In contrast, the cumulative error is largest for FO and PRO. We observe that the cumulative errors are less than 15%, 10%, 10%, and 50% for the RO, OARO, FO, and PRO cases, respectively. While these errors may be significant for some cases, we find that adopting these simplifications reduces the solution time of the detailed model by roughly a factor of 3.

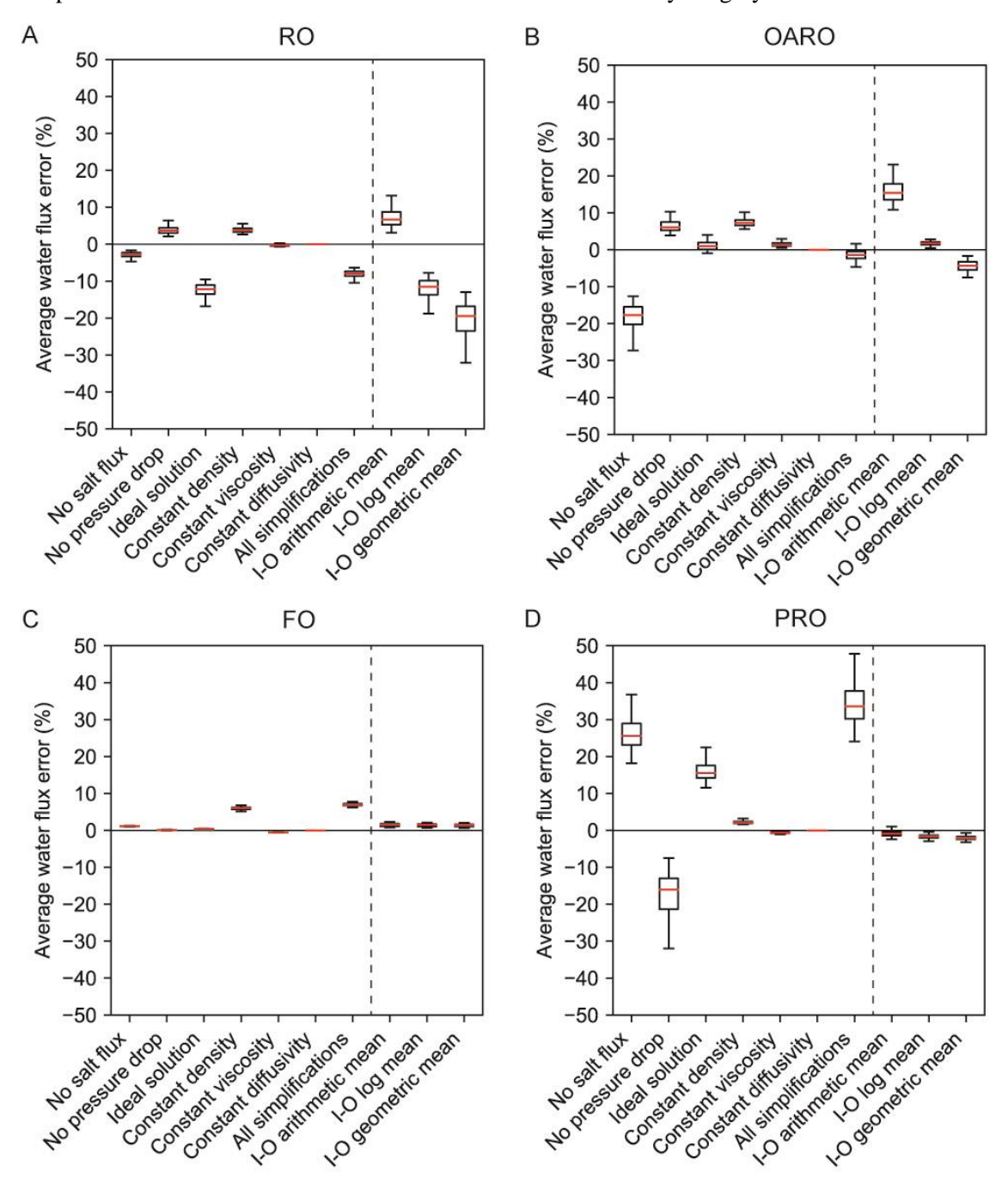


Figure 5. Effect of common simplifications on the accuracy of water flux estimates for the four membrane process case studies: A) RO, B) OARO, C) FO, and D) PRO. All water flux errors are relative to the 10 node finite difference model without employing common simplifications. "All simplifications" includes the no salt flux, no pressure drop, ideal solution, and constant density, viscosity, and diffusivity

assumptions. The right-hand side of the dotted line reports the accuracy of the simplified inlet-outlet (I-O) model formulated with an arithmetic, log, and geometric means.

4.4 Effect of inlet-outlet formulation on model accuracy

In contrast to the process model described above, inlet-outlet models do not directly estimate the profiles of variables along the membrane stage. Instead, they estimate the process performance by averaging the inlet and outlet variables. These models are frequently used because they have reduced computational complexity and are readily incorporated into system-scale optimization models that have higher degrees of freedom. In our work, we find that the inlet-outlet model solves 10 times faster than the detailed model.

We determine the water flux percent error relative to the 10 node finite difference model of the three inlet-outlet modeling formulations. We observe that the arithmetic mean formulation results in large errors (>10%) for the RO and OARO case studies and small errors (<5%) for FO and PRO case studies. Generally, the arithmetic mean overestimates the average water flux for the membrane processes with non-linear water flux profiles.

The log and geometric mean formulations will yield lower average water flux compared to the arithmetic mean. We find that these means underestimate the water flux by up to 40% in the RO case study. In contrast, for the OARO case, the log mean has significantly lower average water flux errors than the geometric or arithmetic means. Finally, in the FO and PRO cases, we find that there is little difference between the means because both cases have relatively flat water flux profiles. When we modify the specifications in the case studies to produce steeper water flux profiles, we find that there is no consistent formulation that results in the lowest error for FO and PRO (Fig. S6). FO and PRO do not have a most accurate formulation because they can be operated with a variety of water flux profiles (e.g. linear or non-linear, increasing or decreasing along the stage), whereas the shape of the water flux profile in RO and OARO are more consistent. Further discussion on the additional FO and PRO case studies are provided in SI section S.5.

One drawback of the log and geometric mean models is that they can incorrectly predict some process configurations as infeasible, meaning that while the target water recovery can be achieved with specified parameters for the detailed one-dimensional model, the water recovery cannot be achieved for the inlet-outlet models. We observe this behavior in 4% and 2% of the Monte Carlo simulations from the RO case study for the log and geometric mean formulations, respectively. The simulations are infeasible for these formulations because they significantly underestimate the average water flux and, thus, overestimate the total membrane area (including membrane length) and total pressure drop. These inflated pressure drops cause the specified water recovery and operating conditions to be infeasible. We do not observe this diverging behavior for the other membrane processes (i.e. OARO, FO, and PRO) because the difference between the water flux at both ends of the membrane stage is significantly smaller.

Collectively, these results suggest that the arithmetic and log mean formulations are the most accurate approaches for inlet-outlet modeling of RO and OARO, respectively. While inlet-outlet modeling can be applied to accurately represent FO and PRO, it is important to begin by using a one-dimensional model to predict the shape of the water flux profile prior to selecting an appropriate mean for estimating the average.

5. Conclusion

While all membrane models are approximations of the process conditions observed in real-world membrane systems, accurate models are critical for developing and predicting the performance of novel membrane technologies. Fully understanding the limitations of existing models and the tradeoffs between model simplicity and model accuracy will further improve our ability to use these models to assess and design novel membrane processes.

This work quantified the errors introduced by common simplifications for the membrane process, solution properties, and modeling. We demonstrated that the finite difference approximation with 10 nodes is sufficient to accurately describe the average water flux to within 0.1%. We also demonstrated that the no salt flux, ideal solution, and constant density simplifications result in the largest water flux errors. Finally, we demonstrated the value of replacing arithmetic mean approximations with a log mean approximation in inlet-outlet models for OARO and FO processes where the water flux is significantly affected by solution conditions on both side of the membrane.

This work has several implications for modeling membrane processes. The first is that the presented finite difference model can be solved efficiently without making common simplifications that are typically rationalized as a means of lowering the computational intensity of the model. Second, the errors resulting from both low node approximations and process and solution property simplifications can result in significant errors in predicted water flux. While these simplifications are specific to the case study parameters, we observe water flux errors as large a 50% for some membrane processes operating under standard conditions. Finally, for applications where simplified inlet-outlet modeling is preferred (e.g. system-scale optimization problems), we have explored the accuracy implications of using different means for all four membrane processes and found that a novel log mean formulation more accurately represents the non-linear water flux in the OARO process.

611 Nomenclature

- 612 Roman symbols
- A Water permeability coefficient [m/bar-h]
- Amem Stage membrane area [m^2]
- B Salt permeability coefficient [m/h]
- C Concentration [g/L]
- Cb bulk concentration [g/L]
- Cm concentration at the membrane interface [g/L]
- D diffusion coefficient of the solute [m²/s]
- d_h Hydraulic diameter [m]
- F Friction factor [-]
- H Channel height [m]
- Js Salt flux [kg/h]
- Jw Water flux $[m^3/m^2-h]$
- k mass transfer coefficient [m/h]
- L Membrane stage length [m]
- M mass flowrate [kg/h]
- *MW* Molecular weight [g/mole]
- N number of nodes
- P Hydraulic pressure [bar]
- PL Pressure loss per unit length [bar/m]
- *Re* Reynolds number [-]
- Rs salt passage [%]
- Rw water recovery [%]
- S structural parameter [m]
- Sc Schmidt number [-]
- Sh Sherwood number [-]
- T Temperature [K]
- W Membrane stage width [m]

- 640 *X* – mass fraction [kg of solute/kg of solution] 641 642 Greek symbols 643 ε – Void space of mesh θ – Inlet and outlet stage variables 644 645 μ – Viscosity [Pa-s] 646 π – Osmotic pressure [bar] 647 ρ – Density [kg/m³] ρw – Pure water density [kg/m³] 648 649 ϕ – Inter-node variables 650 ω – Nodal variables 651 652 Subscript 653 avg – average f – feed-side 654 655 p – permeate-side 656 in – inlet 657 *out* – outlet 658 k – node in set K (k1, k2, ..., kN) 659 660 Miscellaneous $f_{y}(x)$ – function that determines y from variables x 661 662 663 Abbreviations 664 FO – Forward osmosis 665 OARO – Osmotically assisted reverse osmosis 666 PRO – Pressure retarded osmosis RO – Reverse osmosis 667
- 669 Disclaimer

- This manuscript was prepared as an account of work sponsored by an agency of the United States
- 671 Government. Neither the United States Government nor any agency thereof, nor any of their employees,
- makes any warranty, express or implied, or assumes any legal liability or responsibility for the accuracy,
- 673 completeness, or usefulness of any information, apparatus, product, or process disclosed, or represents
- that its use would not infringe privately owned rights. Reference therein to any specific commercial
- product, process, or service by trade name, trademark, manufacturer, or otherwise does not necessarily
- constitute or imply its endorsement, recommendation, or favoring by the United States Government or
- any agency thereof. The views and opinions of authors expressed therein do not necessarily state or
- reflect those of the United States Government or any agency thereof.

Acknowledgements

- We would like to thank Dr. Nick Siefert of the National Energy Technology Laboratory. This work was
- funded via the U.S. Department of Energy's National Energy Technology Laboratory under the
- 683 Crosscutting Technologies Division and via NSF CBET-1554117. Support for T.V.B. was provided by
- appointment to the National Energy Technology Laboratory Research Participation Program, sponsored
- by the U.S. Department of Energy and administered by the Oak Ridge Institute for Science and
- Education. T.V.B. was also supported by the ARCS Foundation Fellowship.

References

- 689 1. Mazlan, N. M.; Peshev, D.; Livingston, A. G., Energy consumption for desalination A
- comparison of forward osmosis with reverse osmosis, and the potential for perfect membranes.
- 691 *Desalination* **2016,** *377,* 138-151.
- 692 2. Sagiv, A.; Zhu, A.; Christofides, P. D.; Cohen, Y.; Semiat, R., Analysis of forward osmosis
- desalination via two-dimensional FEM model. *Journal of Membrane Science* **2014**, *464* (Supplement C),
- 694 161-172.

679 680

687 688

- 695 3. Fimbres-Weihs, G. A.; Wiley, D. E., Review of 3D CFD modeling of flow and mass transfer in
- 696 narrow spacer-filled channels in membrane modules. *Chemical Engineering and Processing: Process*
- 697 *Intensification* **2010**, *49* (7), 759-781.
- 698 4. Bartholomew, T. V.; Siefert, N. S.; Mauter, M. S., Cost Optimization of Osmotically Assisted
- 699 Reverse Osmosis. Environmental Science & Technology 2018, 52 (20), 11813-11821.
- Davenport, D. M.; Deshmukh, A.; Werber, J. R.; Elimelech, M., High-Pressure Reverse Osmosis
- for Energy-Efficient Hypersaline Brine Desalination: Current Status, Design Considerations, and Research
- Needs. Environmental Science & Technology Letters **2018**.
- 703 6. Bartholomew, T. V.; Mey, L.; Arena, J. T.; Siefert, N. S.; Mauter, M. S., Osmotically assisted
- reverse osmosis for high salinity brine treatment. *Desalination* **2017**, *421*, 3-11.
- 705 7. Kim, J.; Kim, J.; Kim, J.; Hong, S., Osmotically enhanced dewatering-reverse osmosis (OED-RO)
- hybrid system: Implications for shale gas produced water treatment. *Journal of Membrane Science* **2018**, 554, 282-290.
- 708 8. Deshmukh, A.; Yip, N. Y.; Lin, S.; Elimelech, M., Desalination by forward osmosis: Identifying
- 709 performance limiting parameters through module-scale modeling. Journal of Membrane Science 2015,
- 710 *491*, 159-167.
- 711 9. Banchik, L. D.; Weiner, A. M.; Al-Anzi, B.; Lienhard V, J. H., System scale analytical modeling of
- 712 forward and assisted forward osmosis mass exchangers with a case study on fertigation. Journal of
- 713 *Membrane Science* **2016**, *510*, 533-545.
- 714 10. Straub, A. P.; Lin, S.; Elimelech, M., Module-Scale Analysis of Pressure Retarded Osmosis:
- 715 Performance Limitations and Implications for Full-Scale Operation. *Environmental Science & Technology*
- 716 **2014,** *48* (20), 12435-12444.
- 717 11. Vince, F.; Marechal, F.; Aoustin, E.; Bréant, P., Multi-objective optimization of RO desalination
- 718 plants. Desalination **2008**, 222 (1), 96-118.

- 719 12. Lu, Y.-Y.; Hu, Y.-D.; Zhang, X.-L.; Wu, L.-Y.; Liu, Q.-Z., Optimum design of reverse osmosis system
- 720 under different feed concentration and product specification. Journal of Membrane Science 2007, 287
- 721 (2), 219-229.
- 722 13. Spiegler, K. S.; Kedem, O., Thermodynamics of hyperfiltration (reverse osmosis): criteria for
- 723 efficient membranes. *Desalination* **1966,** *1* (4), 311-326.
- 724 14. Hoek, E. M. V.; Kim, A. S.; Elimelech, M., Influence of Crossflow Membrane Filter Geometry and
- 725 Shear Rate on Colloidal Fouling in Reverse Osmosis and Nanofiltration Separations. *Environmental*
- 726 Engineering Science **2002**, 19 (6), 357-372.
- 727 15. McCutcheon, J. R.; McGinnis, R. L.; Elimelech, M., Desalination by ammonia–carbon dioxide
- forward osmosis: Influence of draw and feed solution concentrations on process performance. *Journal*
- 729 of Membrane Science **2006**, 278 (1), 114-123.
- 730 16. Yong, J. S.; Phillip, W. A.; Elimelech, M., Coupled reverse draw solute permeation and water flux
- in forward osmosis with neutral draw solutes. *Journal of Membrane Science* **2012**, *392-393*, 9-17.
- 732 17. Scatchard, G.; Hamer, W. J.; Wood, S. E., Isotonic Solutions. I. The Chemical Potential of Water in
- Aqueous Solutions of Sodium Chloride, Potassium Chloride, Sulfuric Acid, Sucrose, Urea and Glycerol at
- 734 25°1. Journal of the American Chemical Society **1938**, 60 (12), 3061-3070.
- 735 18. Pitzer, K. S.; Peiper, J. C.; Busey, R. H., Thermodynamic Properties of Aqueous Sodium Chloride
- 736 Solutions. Journal of Physical and Chemical Reference Data 1984, 13 (1), 1-102.
- 737 19. Mistry, K. H.; Lienhard V, J. H., Effect of Nonideal Solution Behavior on Desalination of a Sodium
- 738 Chloride Solution and Comparison to Seawater. Journal of Energy Resources Technology 2013, 135 (4),
- 739 042003-042003-10.
- 740 20. Washburn, E. W., International Critical Tables of Numerical Data, Physics, Chemistry and
- 741 Technology (1st Electronic Edition). Knovel.
- 742 21. Lobo, V. M. M., Mutual diffusion coefficients in aqueous electrolyte solutions (Technical Report).
- 743 In *Pure and Applied Chemistry*, 1993; Vol. 65, p 2613.
- 744 22. Yip, N. Y.; Tiraferri, A.; Phillip, W. A.; Schiffman, J. D.; Hoover, L. A.; Kim, Y. C.; Elimelech, M.,
- 745 Thin-Film Composite Pressure Retarded Osmosis Membranes for Sustainable Power Generation from
- 746 Salinity Gradients. Environmental Science & Technology 2011, 45 (10), 4360-4369.
- 747 23. Tiraferri, A.; Yip, N. Y.; Straub, A. P.; Romero-Vargas Castrillon, S.; Elimelech, M., A method for
- 748 the simultaneous determination of transport and structural parameters of forward osmosis membranes.
- 749 *Journal of Membrane Science* **2013,** 444, 523-538.
- 750 24. Bui, N.-N.; Arena, J. T.; McCutcheon, J. R., Proper accounting of mass transfer resistances in
- 751 forward osmosis: Improving the accuracy of model predictions of structural parameter. Journal of
- 752 *Membrane Science* **2015**, *492*, 289-302.
- 753 25. Guillen, G.; Hoek, E. M. V., Modeling the impacts of feed spacer geometry on reverse osmosis
- and nanofiltration processes. Chemical Engineering Journal 2009, 149 (1), 221-231.
- 755 26. Chen, J., Comments on improvements on a replacement for the logarithmic mean. *Chemical*
- 756 Engineering Science **1987**, *42* (10), 2488-2489.
- 757 27. Mistry, M.; Misener, R., Optimising heat exchanger network synthesis using convexity properties
- of the logarithmic mean temperature difference. Computers & Chemical Engineering 2016, 94, 1-17.
- 759 28. She, Q.; Jin, X.; Tang, C. Y., Osmotic power production from salinity gradient resource by
- 760 pressure retarded osmosis: Effects of operating conditions and reverse solute diffusion. *Journal of*
- 761 *Membrane Science* **2012,** 401–402, 262-273.
- 762 29. Yip, N. Y.; Tiraferri, A.; Phillip, W. A.; Schiffman, J. D.; Elimelech, M., High Performance Thin-Film
- 763 Composite Forward Osmosis Membrane. *Environmental Science & Technology* **2010,** *44* (10), 3812-3818.
- 764 30. Straub, A. P.; Yip, N. Y.; Elimelech, M., Raising the Bar: Increased Hydraulic Pressure Allows
- 765 Unprecedented High Power Densities in Pressure-Retarded Osmosis. Environmental Science &
- 766 *Technology Letters* **2014,** *1* (1), 55-59.